Porphyrin–Kaolinite as Efficient Catalyst for Oxidation Reactions

Natalia Bizaia,[†] Emerson H. de Faria,[†] Gustavo P. Ricci,[†] Paulo S. Calefi,[†] Eduardo J. Nassar,[†] Kelly A. D. F. Castro,[‡] Shirley Nakagaki,[‡] Katia J. Ciuffi,[†] Raquel Trujillano,[§] Miguel A. Vicente,*[,§] Antonio Gil,[||] and Sophia A. Korili[||]

Universidade de Franca, Franca-SP, Brazil, DQ/Universidade Federal do Paraná, Paraná, Brazil, GIR-QUESCAT, Departamento de Química Inorgánica, Universidad de Salamanca, Salamanca, Spain, and Departamento de Química Aplicada, Universidad Pública de Navarra, Pamplona, Spain

ABSTRACT The preparation, characterization, and application in oxidation reactions of new biomimetic catalysts are reported. Brazilian São Simão kaolinite clay has been functionalized with [*meso*-tetrakis(pentafluorophenyl)porphinato]iron(III), Fe(TPFPP). To obtain the functionalized clay, the natural clay was purified by dispersion–sedimentation, expanded by insertion of dimethyl sulfoxide (DMSO), and functionalized with amino groups by substitution of DMSO with ethanolamine. These previous steps allowed clay functionalization with Fe(TPFPP), leading to a layered material with a basal spacing of 10.73 Å. Clay functionalization with the porphyrin was confirmed by formation of the secondary amine, as demonstrated by FTIR bands at 3500–3700 cm^{-1}. UV–vis spectroscopy revealed a red shift in the Soret band of the iron porphyrin in the functionalized material as compared to the parent iron porphyrin catalyst in solution, indicating $Fe^{III}P \rightarrow Fe^{II}P$ reduction. The catalytic performance of the functionalized clay was evaluated in the epoxidation of cyclooctene, with complete selectivity for the epoxide (100% epoxide yield), and ketonization of cyclohexane, cyclohexanone being the major product. The novel catalyst was also evaluated in the Baeyer–Villiger (BV) oxidation of cyclohexanone, with 85% conversion of cyclohexanone in ε-caprolactone, with total selectivity to ε-caprolactone.

KEYWORDS: kaolinite • functionalization • hybrid materials • porphyrin • heterogeneous catalysis • green oxidation.

1. INTRODUCTION

The preparation, characterization, and application of new catalysts with properties similar to those of the active sites of enzymes comprise a research area known as bioinspired or biomimetic catalysis. There has been considerable growing interest in the use of metalloporphyrins as biomimetic catalysts in recent years (1). Special attention has been focused on the ability of metalloporphyrins to act as models of cytochrome P450 monooxygenases by selectively catalyzing several oxidation reactions of organic and inorganic compounds, under mild conditions (1–3). Metalloporphyrins are also useful building blocks for the design and synthesis of molecular-based solids. The use of hydrogen bonding or metal ion coordination provides a wide range of solid frameworks (4).

Although very efficient homogeneous catalytic systems based on metalloporphyrins have been developed for hydrocarbon hydroxylation and epoxidation, problems such as the oxidative degradation of the catalysts by interaction with the substrates remain unsolved. One approach to minimizing metalloporphyrin degradation is its immobilization in an adequate support (1–3), which provides site isolation of the metal center, thus minimizing catalyst self-destruction and dimerization of unhindered metalloporphyrins (5).

Several materials, such as alumina (6), bentonites (7), montmorillonites (8), polystyrene (9), and silica (10), have been reported in the literature as supports for the preparation of metalloporphyrin heterogeneous catalysts. In these matrices, immobilization of the metalloporphyrin is obtained by polymerization, simple adsorption of an ionic metalloporphyrin, axial ligation of the metal, covalent binding of the metalloporphyrin to the support, intercalation of the metallo complex into layered mineral clay, metalloporphyrin adsorption on the surface of solid matrices, or metalloporphyrin entrapment inside the pores of porous solids (5, 11).

In this context, we have previously reported the successful anchoring of iron and manganese porphyrins onto several supports such as silica and alumina, as well as the use of the obtained solids as catalysts for hydrocarbon oxidation using hydrogen peroxide or iodosylbenzene as oxidants (6, 10).

Even though various approaches to metalloporphyrin immobilization have been considered, progress is still required to further improve metalloporphyrin-based catalytic systems for use in industries regarding the green chemistry context. Major drawbacks of conventional supported catalysts such as low stability, catalyst leaching, and restricted accessibility of the reactants to the reactive centers, as well as catalyst recovery and reuse, must be overcome. Catalyst stability is essential to recycling procedures and to the recovery of valuable metalloporphyrins (12).

* To whom correspondence should be addressed. E-mail: mavicente@usal.es.
Received for review August 21, 2009 and accepted October 26, 2009
[†] Universidade de Franca.
[‡] DQ/Universidade Federal do Paraná.
[§] Universidad de Salamanca.
[||] Universidad Pública de Navarra.
DOI: 10.1021/am900556b

The use of modified clays as catalyst supports in the oxidation of organic compounds has been encouraged, because these systems lead to low waste generation. Moreover, they enable the use of mild conditions and the design of highly selective and active heterogeneous catalysts, which is desirable in an age when the control of environmental pollution and the reduction of energy consumption are mandatory. Moreover, some kinds of clays such as kaolinite provide the advantage of their relatively easy functionalization with organic groups by host−guest interactions. Thus, functionalization of kaolinite is based on the substitution of previously intercalated molecules by others of greater interest, followed by formation of covalent bonds (13).

A variety of organic molecules have been grafted onto the interlayer surface of kaolinite through a covalent link with the inner aluminol groups of the clay. This method has proven to be a useful route for the preparation of hybrid materials and can be interesting for the synthesis of heterogeneous metalloporphyrin catalysts covalently bound to the clays, thereby avoiding catalyst leaching and improving its reuse. In this sense, the grafting of organic groups such as amino can potentially function as a binding site for clay functionalization with second-generation metalloporphyrin bearing several electron-withdrawing substituents at each meso-aryl position, as in the case of Fe(TPFPP) ([*meso*-tetrakis(pentafluorophenyl)porphinato]iron(III)) and Fe(TDCPP) ([*meso*-tetrakis(2,6-dichlorophenyl)porphinato]iron(III)).

Although synthetic metalloporphyrin catalysts have been studied in several oxidation reactions mimicking P450, only a few studies have been devoted to the use of these systems as biomimetic catalysts of enzymes such as the Baeyer−Villiger (BV) monooxygenases (14, 15), which catalyze this reaction in nature. The BV oxidation of ketones is a reaction of considerable interest in organic chemistry because the products, lactones or esters, are important synthetic intermediates in the agrochemical, chemical, and pharmaceutical industries. The oxidants used in the traditional BV oxidation are organic peracids, which potentially produce large amounts of harmful wastes. Much recent effort has been devoted to finding chemically green oxidants and recyclable catalysts (14). The use of supported catalysts together with hydrogen peroxide as oxidant, in particular, leads to environmentally friendly systems, since easy separation of the products and catalyst reuse are allowed, with both operational and economic advantages. Recently, numerous research groups have focused on the study of this reaction in the presence of various catalysts such as aluminas, clays, and transition metals based on several matrices (14, 16, 17).

The aim of the present work is the preparation and catalytic application of a Brazilian kaolinite functionalized with a second-generation metalloporphyrin, Fe(TPFPP). For simplicity, we will refer to the porphyrin used in this work, Fe(TPFPP), as FeP. Clay functionalization was achieved by successive treatments with dimethyl sulfoxide (DMSO), displaced by ethanolamine, and this solid was grafted by FeP. The obtained catalyst was used in green oxidation reactions, namely the epoxidation of cyclooctene and ketonization of cyclohexane, as well as in the BV oxidation of cyclohexanone.

2. EXPERIMENTAL SECTION

2.1. Materials. The clay used in the present work is kaolin from the deposit of São Simão, São Paulo State, Southwestern Brazil, kindly supplied by the mining company Darcy R. O. Silva & Cia. (São Simão-SP, Brazil). Natural clay was purified by means of the dispersion−decantation method (see the Supporting Information); the purified clay is composed of very pure kaolinite and is hereafter designated "Ka".

All solvents and reagents were of high-purity commercial grade (Merck and Aldrich), and most of them were used as received. Dichloromethane (DCM) was dried over anhydrous $CaCl_2$ for 2.5 h, filtered, distilled over P_2O_5, and stored over 4 Å molecular sieves. Pyrrole was distilled under reduced pressure immediately before use. *N*,*N*-Dimethylformamide (DMF) was stirred over KOH at room temperature overnight, decanted, and then distilled at reduced pressure. The purity of (*Z*)-cyclooctene was determined by gas chromatography, and it was purified by column chromatography on basic alumina immediately prior to use.

2.2. Synthesis of the Catalysts. 2.2.1. ***Preparation of DMSO−Kaolinite.*** Intercalation of kaolinite with DMSO was carried out by mixing purified kaolinite (27 g) with DMSO (100 mL) and distilled water (20 mL). The suspension thus obtained was stirred for 10 days at 60 °C (18−20). Then, the clay was separated by centrifugation, washed with ethanol, and dried at 50 °C. This material was designated "Ka-DMSO".

2.2.2. ***Preparation of Ethanolamine−Kaolinite.*** Grafting of ethanolamine onto Ka-DMSO was carried out by refluxing a suspension containing Ka-DMSO (2 g) and ethanolamine (100 mL) for 24 h. The resulting solid was separated by centrifugation, washed with ethanol, dried at 50 °C (21, 22), and hereafter designated "Ka-et".

2.2.3. ***Preparation of [meso-Tetrakis(pentafluorophenyl)porphinato]iron(III) ([Fe(TPFPP)]Cl).*** First, the free base porphyrin, H_2(TPFPP), where TPFPP is a *meso*-tetrakis(pentafluorophenyl)porphinato divalent anion, was prepared according to the procedure reported in the literature (23), producing the porphyrin with a yield of 42%. Its purity was evaluated by its UV−vis spectrum, in a dichloromethane (DCM) solution, where absorption was observed at λ_{max} 410 (Soret band), 508, 582, and 630 nm.

Insertion of iron into the free base porphyrin H_2(TPFPP) was performed by refluxing 50 mg (0.05 mmol) of the free base protonated porphyrin with 250 mg (1.97 mmol) of iron(II) chloride in 10 mL of dimethylformamide (DMF), under an argon atmosphere, according to a method in the literature (24). The iron porphyrin was obtained in its chloride form, [Fe(TPFPP)]Cl, with a yield of 95%. Its purity was evaluated by UV−vis spectroscopy, also in DCM solution: λ_{max} 352, 412 ($\varepsilon = 1.8 \times 10^5$ mol^{-1} L cm^{-1}, Soret band), 504 ($\varepsilon = 1.7 \times 10^4$), 576, and 630 nm.

2.2.4. ***Preparation of Iron Porphyrin Kaolinite Catalyst.*** A mixture of 16 mg of [Fe(TPFPP)]Cl (1.50×10^{-5} mol) and Ka-et (600 mg) in DMF (60 mL) was submitted to reflux and stirred for 48 h under an argon atmosphere. Then, the mixture was slowly cooled and aged overnight in the mother liquor, at room temperature. The solvent was then slowly removed in a rotary evaporator. The obtained solid, designated "Ka-FeP", was washed with dichloromethane and dried at 130 °C for 3 h. The amount of FeP leached from the support was quantified by measuring the amount of FeP in the successive washings by UV−vis spectroscopy. Thus, the percentage of FeP in this catalyst, ignoring the possible variation in the

degree of hydration of the solid in the several steps of the synthesis procedure, was 2.6% (m/m).

In order to test whether FeP can incorporate into the clay without carrying out all the synthesis steps described above, suspensions of FeP and Ka or Ka-et solids were stirred for 3 h and then washed with DCM and dried at 120 °C. In both cases, total leaching of the FeP complex was observed, clearly confirming the importance of the synthesis procedure used for the preparation of a functionalized catalyst. Although these solids do not contain FeP, they were submitted to catalytic tests and denoted as "FeP/Ka" and "FeP/Ka-et", respectively.

2.2.5. *Preparation of Other Iron Porphyrin Catalysts.* For comparative purposes, other catalysts containing Fe(TPFPP) were prepared from various supports.

2.2.5.1. *Supported Fe(TPFPP)/Silica Catalyst.* A 0.7 mL portion of TEOS, 8.50 mL of isopropyl alcohol, and 1.15 mL of ammonia were hydrolyzed in the presence of 1.00×10^{-5} mol of [Fe(TPFPP)]Cl, with magnetic stirring at room temperature. After 30 min of stirring, the solvent was evaporated at room temperature for 1 week, and then the solid was dried at 65 °C. This solid was designated "FeP/Si".

2.2.5.2. *Supported Fe(TPFPP)/Aluminosilicate Catalyst.* A 10 g portion aluminum chloride and 16 mL of diisopropyl ether were reacted in the presence of [Fe(TPFPP)]Cl (1.40×10^{-5} mol, 14.92 mg), in dry DCM (50 mL, previously distilled), with reflux at 110 °C, under an argon atmosphere, for 1 h. The resulting material was reacted with TEOS (3 mL), and then the solvent was removed under vacuum. The solid was washed with several solvents in the order DCM, acetonitrile, and methanol and dried at 65 °C. This solid was designated "FeP/AlSi".

2.3. Characterization Techniques. X-ray diffraction (XRD) patterns of non-oriented powder samples were obtained on a Siemens D-500 diffractometer with Ni-filtered Cu Kα radiation, at 40 kV and 30 mA, at a scanning rate of 2°/min.

FT-IR spectra were recorded in the 350−4000 cm^{-1} range in a Perkin-Elmer 1730 infrared Fourier transform spectrometer, using the KBr pellet technique. About 1 mg of sample and 300 mg of KBr were used in the preparation of the pellets.

Thermogravimetric analysis (TGA) and differential thermal analysis (DTA) were carried out in a Thermal Analysis TA instrument SDT Q 600 simultaneous DTA-TGA-DSC from 25 to 1000 °C, under a nitrogen atmosphere, at a heating rate of 20 °C/min.

Specific surface areas were determined by applying the BET method (25) to the corresponding nitrogen adsorption isotherms, obtained by using a Micrometrics ASAP 2020 physical adsorption analyzer. The samples were previously degassed for 1 h at room temperature, at a pressure lower than 50 μmHg. The nitrogen adsorption data were obtained using 0.2 g of the sample.

Electronic spectra of the materials were recorded with a Hewlett-Packard 8453 diode array UV−vis spectrophotometer. The spectra of the solids suspended in DCM were recorded in a 2.0 mm path length cell. DCM was used as solvent because it led to improved UV−vis spectra when the suspension was prepared. The spectra were preprocessed by using a wavelet filter with Dubauchie (db4) base function for noise minimization, subtraction of the isotonic medium spectrum, multiplicative scattering correction (MSC) to minimize Rayleigh scattering due to variation in the refraction index of the matrix, and a second-degree polynomial fit to minimize matrix fluorescence.

Electron paramagnetic resonance (EPR) measurements of the powder materials were accomplished with a Bruker ESP 300E spectrometer operating at X-band (ca 9.5 GHz), −198 °C, using liquid N_2. The EPR spectra of the solids were recorded after adding the dry material to an EPR quartz tube.

Scanning electron microscopy (SEM) of the materials was performed with a Zeiss DSM 960 digital scanning microscope. The samples were coated with a thin gold layer by evaporation using a Bio-Rad ES100 SEN coating system. Transmission electron microscopy (TEM) was performed using a Phillips CM 200 transmission electron microscope. Specimens for TEM analysis were prepared by grinding the material into fine particles, which were subsequently deposited on carbon-coated palladium films supported on 300 mesh capped grids.

2.4. Catalytic Performance. 2.4.1. *Oxidation Reactions.* Iodosylbenzene was first obtained through hydrolysis of iodosylbenzene diacetate (26); the purity of the obtained compound was evaluated by iodometric titration (27). Iodosylbenzene (0.023 mmol) was added to a 4.0 mL vial sealed with a Teflon-coated silicone septum containing the catalyst (10 mg), 1,2-dichloroethane (1 mL), (*Z*)-cyclooctene, previously purified on alumina column, or cyclohexane as the substrate (1.15 mmol) and di-*n*-butyl ether as an internal standard (10 μL). The reaction products were analyzed by gas chromatography. These analyses were carried out on an HP 6890 chromatograph equipped with a hydrogen flame ionization detector and capillary column (HP-INNOWax-19091N-133, polyethylene glycol length 30 m, internal diameter 0.25 μm). The products were quantified using a calibration curve obtained with a standard solution, and the yields were based on the added oxidant, iodosylbenzene.

The BV oxidation reaction was carried out in a 4.0 mL glass reactor. A 50 μL portion of cyclohexanone (0.48 mmol), 850 μL of benzonitrile (7.95 mmol), 5.0 μL of di-*n*-butyl ether (2.94 μmol), 176 μL of 60 wt % hydrogen peroxide (4.53 mmol), and 20 mg of the catalyst were added to the reactor; the mixture was then heated to 80 °C and stirred for 48 h. The reaction products were analyzed by gas chromatography (HP 6890).

In both cases, a control of the reaction was carried out in the absence of catalyst.

2.4.2. *Reuse of the Catalysts.* At the end of the reaction, the Ka-FeP catalyst was recovered by centrifugation and washed 5 times with 1 mL of methanol, to ensure that any remaining iodosylbenzene would be removed from the catalyst. The catalyst was then dried for 3 h at 60 °C, before being used again in (*Z*)-cyclooctene oxidation.

In the BV oxidation, the catalyst was recovered by centrifugation and then dried for 3 h at 65 °C, before being used again.

2.4.3. *Catalytic Intermediates from Ka-FeP and Iodosylbenzene.* The experiment was adapted from ref 28. Briefly, the intermediates from the reactions between Ka-FeP and iodosylbenzene were studied by initially placing 100 mg of Ka-FeP and 450 μL of dichloroethane in a quartz cell (path length 2 mm). After sinking of the Ka-FeP, the cell was transferred to a homemade low-temperature optical Dewar flask containing methanol previously cooled to −55 °C, and the spectrum of the Ka-FeP suspension was recorded. Next, 0.023 mmol of PhIO in 150 μL of dichloroethane was added to the cell and the mixture was stirred. The cell was placed in the optical Dewar and the suspension was left to stand again, until the Ka-FeP was totally sunk. The UV−vis spectra were recorded. The Ka-FeP and iodosylbenzene mixture was stirred every 20 min, until 80 min of reaction.

3. RESULTS AND DISCUSSION

3.1. Characterization of the Materials. As indicated before (29), purification of natural kaolin by dispersion−decantation gave rise to a very pure kaolinite. Its basal spacing is 7.14 Å, and all the characterization data are in accord with very pure kaolinite (see the Supporting Information).

Kaolinite was initially treated with DMSO, in order to expand its layers and enable the later insertion of other molecules. The DMSO-treated sample has a basal space of 11.20 Å; thus, the expansion of the interlayer space produced by the incorporation of DMSO molecules is 4.06 Å,

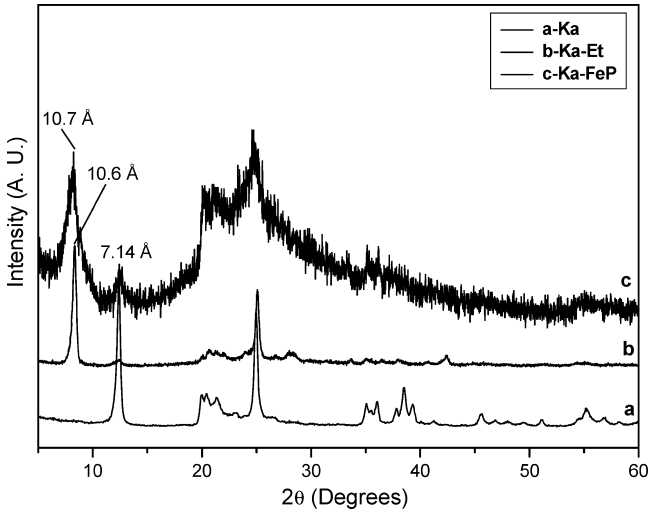

FIGURE 1. X-ray powder diffraction patterns of Ka (a), Ka-et (b), and Ka-FeP (c).

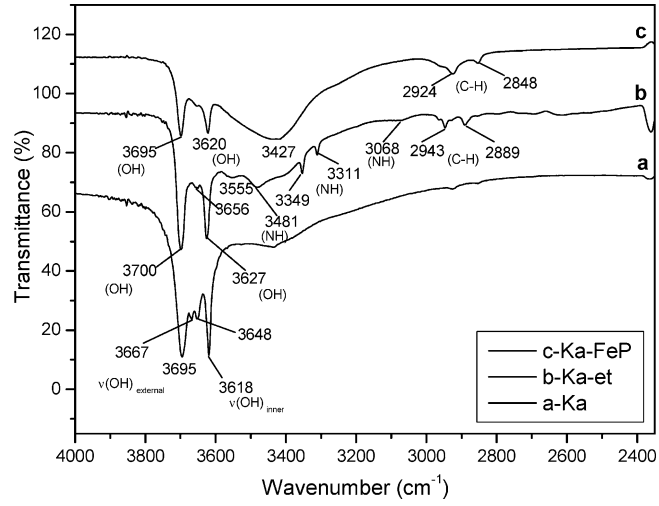

FIGURE 2. Infrared absorption spectra, high-wavenumber region, of Ka (a), Ka-et (b), and Ka-FeP (c).

which agrees with literature data (30−32) and demonstrates excellent expansion of the clay, as confirmed by all the characterization techniques. This reaction has been extensively reported in the literature (33). Recently, we have expanded São Simão kaolinite with DMSO as a first step in the functionalization of this clay with carboxylic acids derived from pyridine (20); details on the characterization of this solid can be found in ref 20, and some data are included now in the Supporting Information.

The expansion of kaolinite with DMSO allowed the insertion of a new guest molecule, ethanolamine, by displacement of DMSO. The basal spacing of the Ka-et solid is 10.6 Å (Figure 1), slightly lower than that of Ka-DMSO because of the orientation of the molecules but clearly larger than in the original kaolinite. It is observed that the peak at 11.2 Å completely disappears, which suggests the complete substitution of DMSO by ethanolamine and the effective functionalization of kaolinite with the latter compound. In fact, this hypothesis has been confirmed by other techniques.

The X-ray diffractogram of the solid functionalized with FeP is shown in Figure 1, where it is compared with the diffractogram of the parent kaolinite and the Ka-et solid intermediate used for its preparation. The interlayer space was maintained in relation to Ka-et, but the X-ray diffraction shows the amorphization of the solid, as evidenced by the widening of the peaks compared with the solid functionalized with ethanolamine. This demonstrates that FeP was incorporated into the interlayer space of the solid, which is also confirmed by other techniques. The functionalization of the clay with FeP was based on the property of the pentafluorophenyl substituents in this metallo complex to react with the nucleophile NH_2 groups of the previously fixed ethanolamine, with selective substitution of the −F substituents in the para position of the meso-aryl groups (34).

In comparison to the bands in the spectrum of kaolinite (Supporting Information), the bands at high wavenumbers in the FTIR spectrum of the Ka-et solid are shifted (Figures 2 and 3). The band corresponding to the internal hydroxyls (3618 cm^{-1} in kaolinite) shifts to 3627 cm^{-1}, while the vibration at 3696 cm^{-1} in Ka shifts to 3691 cm^{-1} in Ka-et. These shifts are characteristic of clay functionalization with amine groups (21, 22). At the same time, other typical bands of amino group vibrations are found at 3068, 3311, and 3355 cm^{-1}, whereas bands typical of C−H bonds are detected at 2940 and 2885 cm^{-1} (21, 22). Vibrations at 3200 and 1625 cm^{-1} are characteristic of N−H bonds, thereby confirming the grafting reaction between the amine groups and the surface of kaolinite (21, 22).

The band corresponding to inner Al−OH vibrations at 912 cm^{-1} (see Figure 3) also shifts to 900 cm^{-1} upon reaction, which is further evidence of the functionalization of kaolinite with ethanolamine. The band characteristic of surface Al−OH vibrations in Ka at 938 cm^{-1} shifts to 974 cm^{-1} upon reaction, indicating that the outer hydroxyl groups of kaolinite are also functionalized, as previously reported by Detellier et al. (21, 22). Thus, ethanolamine molecules functionalize both the interlamellar space and the surface of kaolinite. Vibrations at 1006 and 1045 cm^{-1} are also typical of ethanolamine incorporation into the kaolinite matrix, revealing that a strong interaction takes place (21, 22).

The band characteristic of the amine group at 3481 cm^{-1} is displaced to 3425 cm^{-1} (see Figure 2), a consequence of the interaction of the fluoro substituents on FeP with the NH_2 groups present in the clay functionalized with ethanolamine. The two sharp N−H stretching bands at 3349 and 3311 cm^{-1} are not observed in the solid functionalized with FeP, while C−H stretching bands are detected at 2946 and 2889 cm^{-1} (21, 22). Thus, the reaction between Ka-et and FeP and the subsequent intercalation of FeP into the interlayer region of kaolinite are shown in Scheme 1. It is noteworthy that this reaction must be carried out at temperatures around 150 °C, as obtained in refluxing DMF, since it has been previously reported that it does not occur at lower temperatures (34, 35). DMF was bubbled with argon prior to the functionalization reaction, to avoid its decomposition into dimethylamine, which could lead to complicating side reactions where dimethylamine could act as a nucleophile, thus competing with the amino groups on the matrix in the halogen substitution reaction.

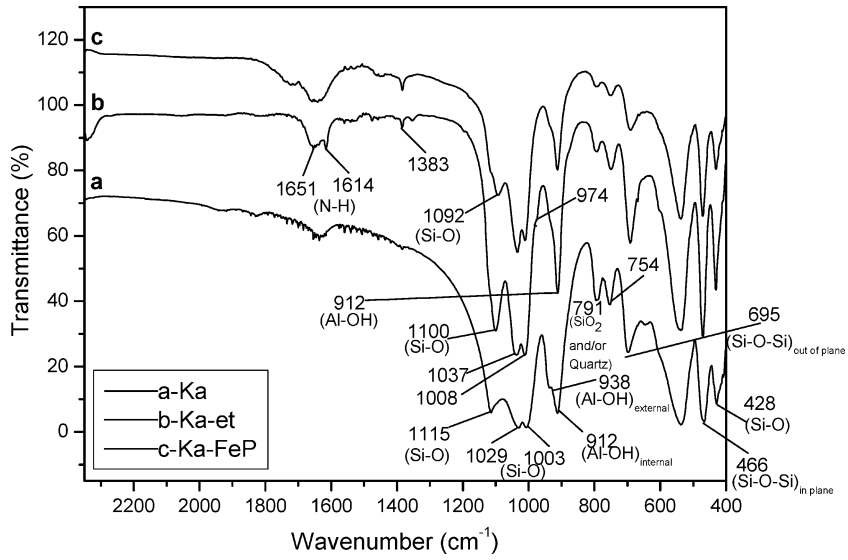

FIGURE 3. Infrared absorption spectra, low-wavenumber region, of Ka (a), Ka-et (b), and Ka-FeP (c).

Scheme 1. Schematic Representation of the Functionalization of Ka-et with Fe(TPFPP)

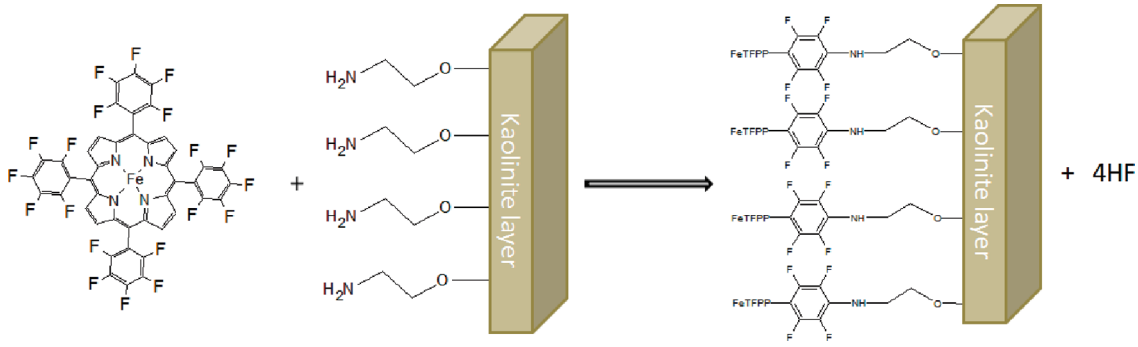

The porphyrin ring exhibits characteristic absorbance properties in the UV−vis region: it has an intense absorption near 400 nm ($\varepsilon \approx 10^5$ mol^{-1} L cm^{-1}), referred to as the Soret band, which is characteristic of the macrocyclic systems, and it is normally the band of choice for spectrophotometric determinations (36). The UV−vis spectrum of the FeP−ethanolamine functionalized kaolinite displays a Soret band at 422 nm, which is red-shifted compared to FeP in solution: 411 nm (Figure 4). This suggests that the Fe(III)/Fe(II) reduction process has taken place, because of bis-coordination of the NH_2 groups on the support to FeP. Another explanation for this shift could be the fact that FeP is located in a very confined space, as in the case of metalloporphyrins inside zeolites or glasses (37). Preliminary EPR analysis showed $g \approx 6$, typical of high-spin Fe(III), and could not indicate whether part of the Fe(III) sites have actually been reduced to Fe(II), since the latter are EPR silent.

EPR analysis of Ka-et and Ka-FeP materials are shown in Figure 5. The EPR spectrum of the kaolinite−ethanolamine material (Figure 5A) revealed the presence of a component, in small amounts, at $g = 4.3$ (intensity 7000), attributed to various iron species in rhombic symmetry, which are frequently present in natural clays and had been previously observed in chemical analyses of the kaolinite clay used here (37). The EPR spectrum of Ka-FeP (Figure 5B) displays a more intense signal at $g = 4.3$ (intensity 40 000) in comparison with the spectrum of the Ka-et solid. A broad signal in the region of $g = 2$ is also observed, which can be attributed to Fe−Fe couplings (38). Thus, on the basis of the EPR experiments, we can conclude that FeP is located in a very confined space in the clay.

SEM micrographs of the Ka-et and Ka-FeP solids are very different (Figure 6). The shapes of the particles change considerably; they agglomerate in the presence of FeP, giving rise to large and spongy particles. This may be related to the creation of hydrophilic regions in the environment of each particle, which promotes the aggregation of new ones.

Figures 7 and 8 show the thermal curves of the Ka-et and Ka-FeP samples, respectively. First, it should be indicated that original kaolinite (see the Supporting Information) undergoes loss of adsorbed water as a weak endothermal effect at 65 °C, as well as loss of structural water, derived from the decomposition of hydroxyl groups with formation of the phase known as metakaolinite, as an endothermal effect at 520 °C (21, 22, 30, 39). In the high-temperature region, the structural reorganization of the material, with nucleation of mullite, is observed as an exothermal process close to 1000 °C (21, 22).

The thermal curves of the Ka-DMSO sample (not shown) showed the typical behavior of this complex (20). The observed mass loss allowed calculation of the amount of

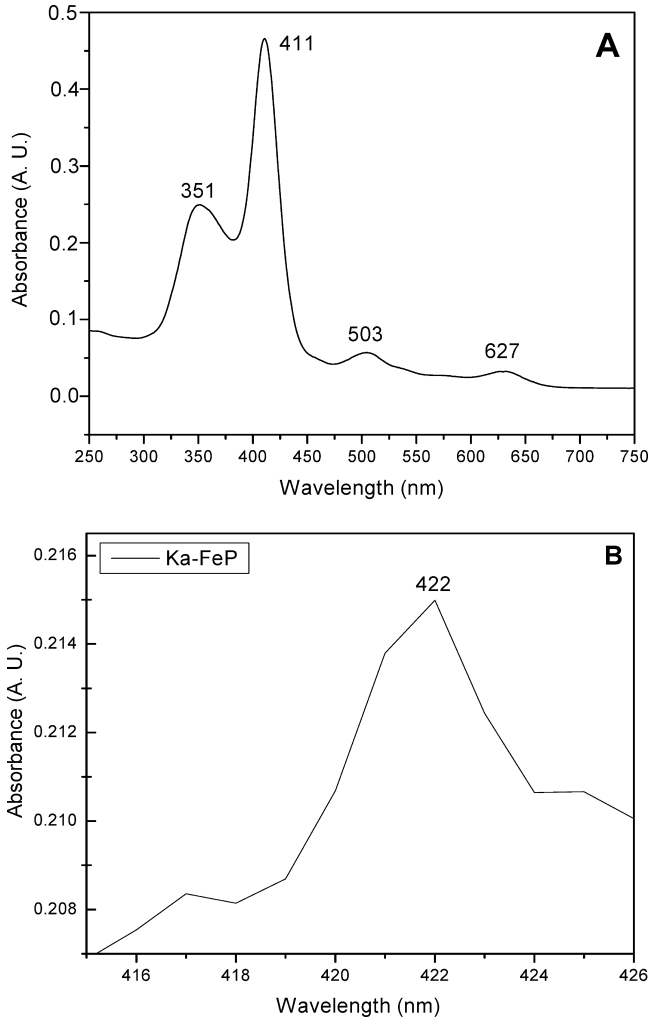

FIGURE 4. UV−vis spectra of Fe(TPFPP) in solution (A) and in solid Ka-FeP (B).

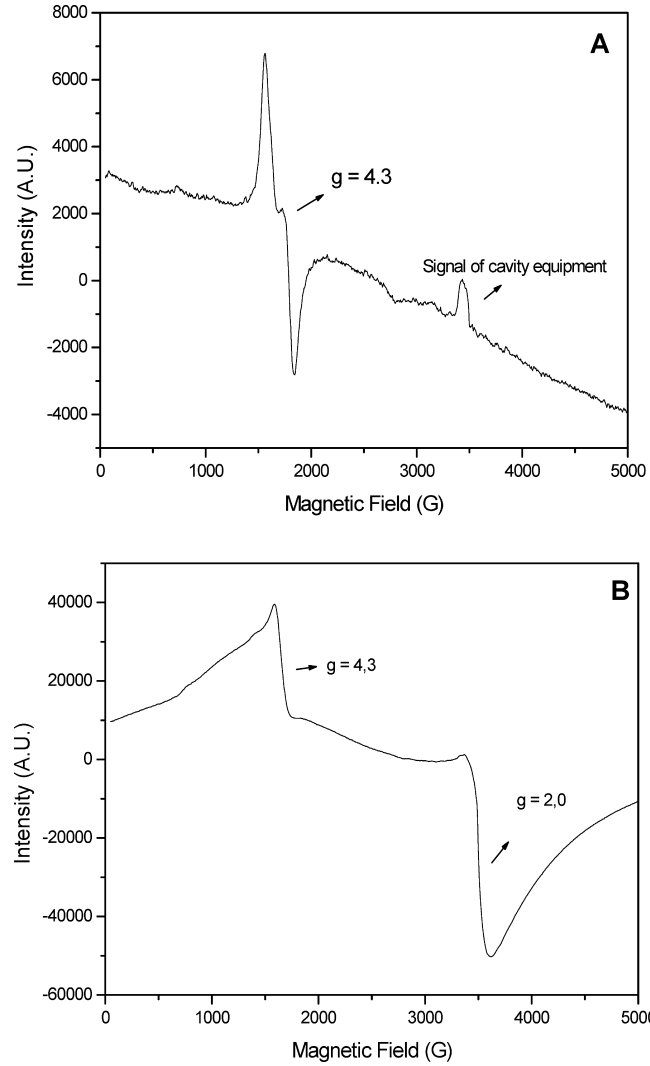

FIGURE 5. EPR spectra of Ka-et (A) and Ka-FeP (B) solids. Conditions: temperature, 4 K; microwave power, 20 mW; modulation amplitude, 4.0 GHz; gain, 500.

DMSO fixed by the solid, leading to a stoichiometry of Ka-$(DMSO)_{0.448}$.

The TG curve of Ka-et (Figure 7) displays two intense mass loss steps, centered at 220 and 550 °C. The detailed analysis of the curve by means of its derivative shows a first mass loss step actually composed of two processes. The second mass loss step, composed of three processes centered at 211, 303, and 390 °C, is assigned to the elimination of ethanolamine molecules intercalated into the mineral clay layers. The first process, which is much more intense, may be due to the removal of the more easily accessible ethanolamine molecules, while the other two are due to less accessible molecules and/or ethanolamine very strongly bound to the inorganic matrix. In fact, there is not true separation between these last processes. The dehydroxylation of kaolinite is centered at 476 °C; the intercalation makes the dehydroxylation take place 44 °C below this same process in the case of pure kaolinite. All the processes are slightly endothermal. The total mass loss from room temperature to 1000 °C is 29% of the initial weight of the sample, while the mass loss between 165 and 410 °C, the interval in which the loss of ethanolamine can be situated, is 13.8%. This value allows us to calculate the stoichiometry of the formed complex, which is Ka-$(et)_{0.64}$.

Thermal analysis of the solid Ka-FeP is shown in Figure 8. Small amounts of adsorbed water and perhaps solvent are removed below 200 °C. The loss of organic matter, namely ethanolamine and porphyrin, is observed as an endothermal effect centered at 370 °C, followed by kaolinite dehydroxylation. The DTG curve reveals an interesting endothermal effect centered at 639 °C, which can be tentatively assigned to the elimination of residual carbon trapped in the kaolinite matrix or to changes in the oxidation state of the Fe ion. The oxide of this element that is stable at high temperature is the spinel; in addition, spinels involving Al from kaolinite may also be formed. The thermal stability of the kaolinite-FeP adduct up to a temperature as high as 370 °C is highly remarkable. The profile of the curve and also the mass loss are similar to those of the Ka-et solid, as may be expected because of the low amount (2.6%) of FeP incorporated into the solid. In this respect, transforming these mass values to moles, the following formula is calculated for the kaolinite−ethanolamine−iron porphyrin com-

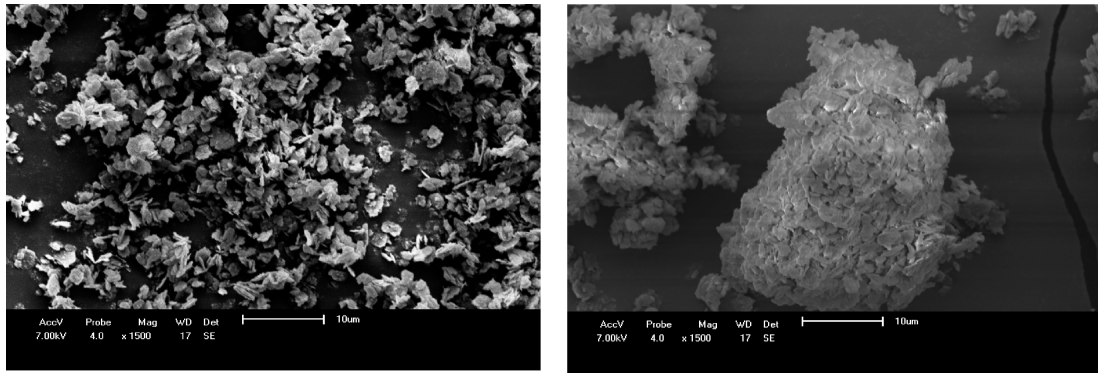

FIGURE 6. SEM images at a magnification of 1500× of Ka-et (left) and Ka-FeP (right) solids.

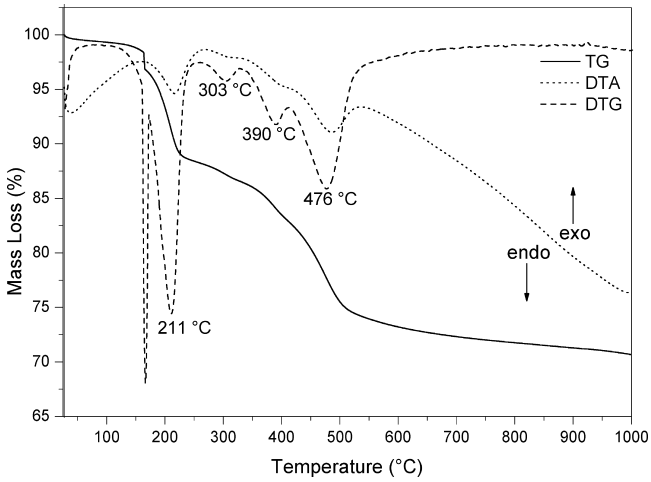

FIGURE 7. Thermal curves of the Ka-et sample, obtained under an N_2 atmosphere.

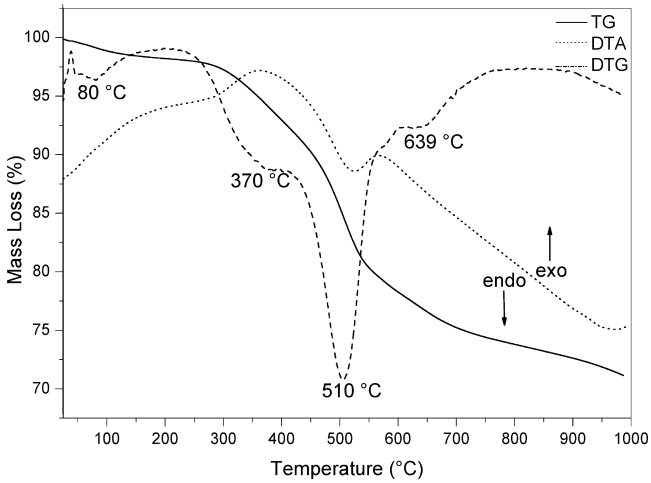

FIGURE 8. Thermal curves of the Ka-FeP sample, obtained under an N_2 atmosphere.

pound: $Ka(et)_{0.64}(FeP)_{0.0067}$. Thus, the ratio iron porphyrin/ethanolamine is found to be 0.0105, ca. 24 times lower than the maximum ratio allowed by the stoichiometric reaction between these compounds, which is 0.25. The latter ratio is calculated by taking into account that in each of the phenyl rings of the porphyrin only the F in a position para with the core of the molecule can react with the amine groups and that there are four of these rings in each molecule, as can be seen in Scheme 2. Probably, steric constraints do not allow all four groups of a molecule to bind to the kaolinite layers, and in fact, in Scheme 2 only one of the groups is bound. Incorporation of higher amounts into the clay interlayer region may be restricted by steric constraints, but this is not at all a negative factor for its catalytic activity. The incorporation of a limited amount of porphyrin, and mainly the fact that these molecules are isolated from the others, may favor the catalytic activity. This is because the active phase is "diluted" into the solid matrix, making the active site of the catalyst more accessible.

The surface area and porosity of the materials, determined from nitrogen adsorption, are summarized in Table 1. Data from purified kaolinite are also included for comparison. In all cases, low values of surface area are found, indicating that the organic species almost completely fill the interlayer space of kaolinite. This effect is mainly observed in the solids treated with DMSO, ethanolamine, and FeP. The number of Brønsted acid sites, determined by retention of cyclohexylamine (40), considerably increased on going from the natural kaolinite (0.21 mmol/g) to the Ka-FeP solid (1.00 mmol/g), which can also be an important factor influencing the catalytic activity of the solids.

With all the data obtained by characterization of the solids, the successive processes involved in the functionalization of the clay may be summarized as indicated in Scheme 2.

3.2. Catalytic Performance. In order to test the catalytic performance of FeP immobilized on kaolinite, the substrate (*Z*)-cyclooctene was submitted to the oxidation reaction using iodosylbenzenene (PhIO) as oxygen donor, in the presence of the Ka-FeP solid, at room temperature and pressure. (*Z*)-Cyclooctene is often used as a diagnostic substrate whenever a new catalytic system is synthesized for various reasons. First, its main oxidation product, cyclooctenoxide, enables easy evaluation of catalyst efficiency because of its stability (41). In addition to that, epoxides are very useful intermediates in the chemical industry, since they are the starting point for the preparation of various products.

Furthermore, PhIO was chosen as the oxygen source because it gives good oxidant conversion, it is relatively inert in the absence of FeP, and its reaction with these catalysts generates the ferryl radical $Fe^{IV}(O)P^{\cdot+}$ and PhI. Moreover, this oxidant is a polymeric solid that does not contain weak

Scheme 2. Schematic Representation of the Synthesis Procedure and the Structure of the Various Solids

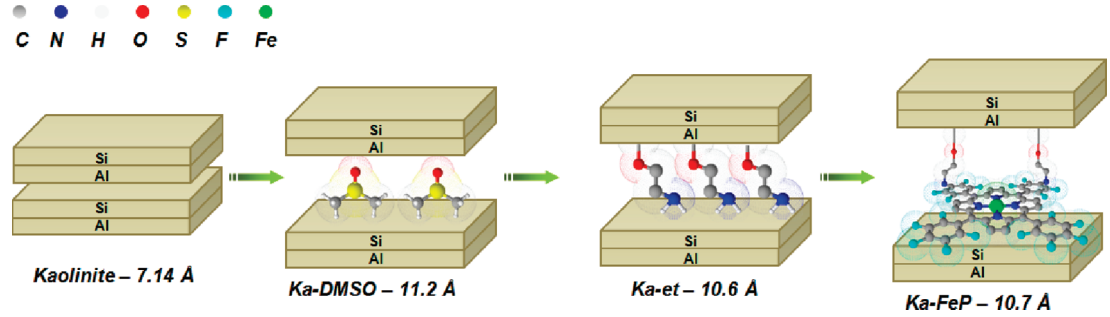

Table 1. Textural Properties of the Samples

sample	BET surface area (m^2/g)	pore volume (cm^3/g)
Ka	19 ± 1	0.103 ± 0.001
Ka-DMSO	4 ± 1	0.085 ± 0.001
Ka-et	16 ± 1	0.090 ± 0.001
Ka-FeP	10 ± 1	0.068 ± 0.001

Table 2. Characteristics of FeP Immobilized in Various Supports and Yield using the Solids Obtained as Catalysts and Iodosylbenzene as Oxidant

catalytic solid	UV−vis Soret band (nm)	FeP loading (%)	yield C-ox[a] (%)[b] 1 h	24 h
Ka-et			0	0
Ka-FeP	422 ± 1	2.6 ± 0.1	100 ± 10	100 ± 10
$[Fe(TPFPP)]^{+}$ [c]	412 ± 1		85 ± 8	85 ± 8
FeP/Si	410 ± 1	2.5 ± 0.1	30 ± 3	50 ± 5
FeP/AlSi	410 ± 1	2.8 ± 0.1	10 ± 1	65 ± 6
FeP/Ka-et			0	0
FeP/Ka			0	0

[a] C-ox = cyclooctenoxide. [b] The yield was based on iodosylbenzene. [c] FeP was used as homogeneous catalyst in solution.

O−H bonds, thus eliminating the occurrence of free radical chain reactions normally initiated by oxidants such as alkyl hydroperoxides, R−O−O−H (42).

The overall accountability for the oxidant was achieved by measuring the iodobenzene (PhI) yield in all the reactions. As PhI yields are almost 100% in all cases, the competitive reaction between PhIO and the active catalytic species ferryl radical, $Fe^{IV}(O)P^{\cdot+}$, probably does not occur in our system (2).

Catalytic results are shown in Table 2. When the Ka-FeP catalyst is employed, 100% epoxide yield is achieved after 1 h of reaction, and no decrease in product yield is detected after 24 h of reaction, suggesting the high stability of the catalytic solid. This activity is superior to that observed using the parent FeP in solution (100% yield; cf. 85% in homogeneous catalysis), giving evidence that immobilization of FeP on the clay improves the catalytic activity of the metallo complex. The differences in the catalytic performance of homogeneous and heterogeneous catalysts may be partly due to differences in the stability of the active catalytic species because of the site-isolation principle (5).

Control reactions, or blank tests, were carried out with the Ka-et matrix containing no FeP and with a solution blank without any solid; these reactions did not lead to any product yield. Blank tests were also carried out in the absence of oxidant, and they did not give any detectable conversion, either. This fact confirms that the observed catalytic activity is really due to the FeP complex.

For comparison purposes, reactions were also carried out with FeP immobilized or adsorbed onto the following supports: (a) silica with spherical particles and (b) synthetic aluminosilicate. The reactions were performed in the presence of solid catalysts containing FeP loadings very similar to that found in the Ka-FeP catalyst. As expected for this second-generation FeP, all the catalysts catalyzed the epoxidation of (*Z*)-cyclooctene by iodosylbenzene, but the epoxide yields were inferior to that observed with Ka-FeP. In contrast to the Ka-et matrix, a fraction of the active sites may be inaccessible to the reactants in the case of the supports Si and AlSi. Alternatively, these supports may create internal diffusion of the reactants, causing extra difficulties.

Despite the low product yield obtained for FeP immobilized on the supports Si and AlSi as compared to kaolinite, the UV−vis spectra of the supernatant solutions obtained after the oxidation reactions using the three solid heterogeneous catalysts revealed that there was no catalyst leaching from the supports in any of the conditions considered here, since the typical FeP Soret band at 412 nm was not detected in such solutions. This fact suggests that immobilization of this FeP on kaolinite, the best catalyst, or even on the other two supports, has the advantage of enabling catalyst reuse.

The FeP solution was also magnetically stirred with either the Ka or the Ka-et solid for incorporation of FeP into these solids, in order to investigate whether the immobilization procedure influenced the catalytic activity. The solids resulting from the incorporation process, FeP/Ka and FeP/Ka-et, respectively, presented total FeP leaching, 100%, during the washing step. It is therefore not surprising that the reactions with these catalysts did not give any epoxide yield. This confirms the importance of the functionalization procedure adopted for the synthesis of the Ka-FeP catalyst.

Table 2 shows that, after only 1 h of reaction, the Ka-FeP catalyst already leads to higher epoxide yield than the other catalysts, which implies a higher initial epoxidation rate in this case. As for the FeP/Si and FeP/AlSi catalysts, maximum epoxide yields were achieved after only 24 h of reaction, but

the yields were clearly lower than that obtained with the Ka-FeP catalyst.

This observation suggests that the higher reaction rate and product yields obtained in the case of Ka-FeP compared to the two other supports are due to the structure of the particles constituting these systems. Also, in the Ka-FeP catalyst the particles are positioned in such a way that substrate access and product diffusion are very much facilitated when kaolinite is employed as matrix, and the catalytic activity of the clay system is thus remarkably higher, as will be discussed in the reuse experiments.

To prove that catalysis is genuinely heterogeneous and to confirm the participation of FeP in the reactions, the catalyst Ka-FeP was filtered off from the reaction mixture, extra oxidant was added to the resulting supernatant, and the oxidation reaction was allowed to proceed under the same initial conditions for another 72 h. After this period, no (*Z*)-cyclooctene oxide yields were observed, indicating that the catalytic activity of the FeP-catalyst materials is truly heterogeneous and FeP plays an essential role in the catalysis.

The high efficiency and stability of the Ka-FeP system can be confirmed via catalyst reuse. For this purpose, the solid catalysts were separated from the reaction mixture after each experiment by simple filtration and dried before being used in a subsequent run. In the case of Ka-FeP, the catalyst was reused in five consecutive runs without any decrease in activity. The epoxide yield was maintained at 100% throughout the five reuse reactions, while for FeP/Si and FeP/AlSi only one recycling cycle was possible, and this reuse led to significantly decreased epoxide yields: for FeP/Si, 20% epoxide yield after the first reuse, 2% epoxide yield after the second, and 0% epoxide yield after the third reuse, while in the case of FeP/AlSi, 21% epoxide yield was found after the first reuse, 4% epoxide after the second, and 0% epoxide yield for subsequent reuse. These results were very similar to those previously observed by us in the case of the FeP/Al system.

Some authors have observed deactivation of the catalysts in the epoxidation reaction and have attributed their results to catalyst leaching or metalloporphyrin dimerization. In fact, it is very often reported in the literature that formation of the active catalytic species $Fe^{IV}(O)P^{\cdot+}$ is difficult when dimeric species are produced (2, 5, 34). In our case, both hypotheses were discarded once no leaching was observed by UV−vis of the supernatant, and the UV−vis spectra of both solids FeP/Si and FeP/AlSi after the first reuse cycle were the same as the respective starting spectrum, before the first reaction. Indeed, it has been reported that immobilization of second- and third-generation metalloporphyrins on inorganic supports can improve the stability of these catalysts against oxidative self-degradation and dimerization, thus leading to better catalytic results (34).

Sacco et al. (43) have observed that in some solvents there is a competition between PhIO and cyclooctene for the active oxidant, resulting in the formation of iodoxybenzene ($PhIO_2$) and a consequent decrease in the epoxide yields. In our case, no formation of $PhIO_2$ was detected by iodometric assay; therefore, as observed by McDonald et al. (12), $PhIO_2$ does not act as deactivator of the catalyst.

McDonald et al. (12) used a heterogeneous silica−manganese−porphyrin as a catalyst for (*Z*)-cyclooctene oxidation by iodosylbenzene and observed that the catalyst became gradually less active over four reuse cycles; after the fifth cycle, the catalyst was completely inactive. These authors attributed the catalyst deactivation to side-product accumulation on the silica surface, which hinders the access of the reactants to the active site in the metalloporphyrin. Alternatively, access to the active site could be blocked due to pulverization of the silica support. In the present work, after the first reuse reaction the materials FeP/Si and FeP/AlSi were transformed into a finer powder compared to the initial material. In fact, porous solids commonly employed in catalysis are found in the form of powders because the mechanical stress of grinding makes them more compact. Apparently, the stirring procedure used during the oxidation reaction fragments the support, resulting in the formation of fine particles in the reaction medium. These particles may block the access to the active sites, thereby leading to lower catalytic yields in the second cycle. It is important to remark that this effect was not observed in the case of the Ka-FeP solid.

Indeed, as observed by Sacco et al. (43), one limitation of the metalloporhyrin heterogeneous reuse procedure is the physical stability of the support to prolonged stirring. Reaction in the presence of the Ka-FeP catalyst was also prolonged up to 72 h, and the quantitative yield of the epoxide, 100%, was maintained within this period. This fact indicates that no competitive reactions took place during this long period and that the catalyst remained active, thus confirming the stability of the immobilized FeP in the clay support. In our case, it is reasonable to propose that the supports prepared by sol−gel methodologies are less stable compared to the clay catalyst.

The ferryl radical, $Fe^{IV}(O)P^{+}$, is described in the literature as the active species responsible for the oxidation carried out by biological enzymes such as cytochrome P-450 (42). Several studies involving oxidation reactions by PhIO in the presence of synthetic iron porphyrins have provided a consensus mechanism where PhIO transfers an oxygen atom with two oxidizing equivalents, to form a high-valent oxo−iron complex, $Fe^{IV}(O)P^{+}$, capable of epoxidizing olefins.

Reaction efficiency depends on the facility for generating this active species and transferring the oxygen atom to the substrate. The results presented in Table 2 suggest that kaolinite contributes to the stabilization of the active species and, as previously observed by Kameyama et al. for cobalt−porphyrin−montmorillonite systems (8), the clay is also responsible for accelerating the epoxidation.

Experiments performed at low temperature to investigate the reaction between Ka-FeP and iodosylbenzene (Figure 9) gave evidence for the formation of the active species $Fe^{IV}(O)P^{+}$. Indeed, a lower intensity of the Soret band characteristic of the metal−oxo species was detected in this

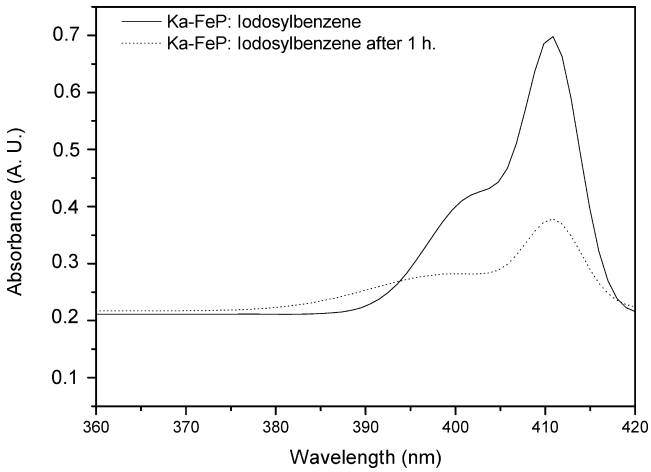

FIGURE 9. UV−vis spectra of the reaction between Ka-FeP and iodosylbenzene after 1 h at low temperature.

reaction. This phenomenon is due to the replacement of the red color of the FeP by the green color typical of the high-valent oxo−iron complex $Fe^{IV}(O)P^{+}$. Iamamoto et al. (28) have already reported on the formation of this active intermediate species in the case of iron porphyrin immobilized on functionalized silica. In the present case, it was possible to visualize the Soret band only, because of the low concentration of FeP in the Ka-FeP system.

In order to confirm whether the high-valent oxo−iron complex $Fe^{IV}(O)P^{+}$ is the only active species responsible for the oxidation reaction when Ka-FeP is used as catalyst, (*Z*)-cyclooctene oxidation reactions were performed in the presence of *tert*-butyl alcohol, a well-known radical scavenger. There were no changes in the epoxide yields in the presence of this compound, thus allowing us to dismiss the radical mechanism.

There is a generalized consensus on the promotion of a number of oxidative biotransformations, including the hydroxylation of inactive hydrocarbons, by the high-valent oxo−iron complex $Fe^{IV}(O)P^{+}$ produced from biological cytochrome P-450 via the rebound mechanism. To confirm the versatility of the intermediates formed in our present system, its efficiency for the oxidation of an inert substrate, namely cyclohexane, was tested. This substrate also enables evaluation of catalyst selectivity because it can generate cyclohexanol and/or cyclohexanone as oxidation products. Another reason for studying cyclohexane oxidation is its great industrial importance; the mixture cyclohexanol/cyclohexanone, the so-called KA-oil, is employed in the synthesis of textile fibers, such as nylon-6 and nylon-6,6 (44).

The use of Ka-FeP as catalyst for cyclohexane oxidation by iodosylbenzene led to a yield of 30%, the product being formed by a mixture of cyclohexanol (14%) and cyclohexanone (16%). Thus, the catalyst is slightly more selective for the ketone (ketone/alcohol = 1.15). Usually, cyclohexanone may be formed via a radicalar mechanism (45), but as mentioned before, the experiments carried out in the presence of a radical scavenger allow us to dismiss the existence of such a mechanism. Thus, it is reasonable to think that the ketone is produced by reoxidation of the alcohol initially

Table 3. Conversion of Cyclohexanone in ϵ-Caprolactone in the Baeyer−Villiger Reaction from Ka-FeP Catalyst and Hydrogen Peroxide as Oxidant

	ϵ-caprolactone (conversion %)[a]			
time(h)	run 1	run 2	run 3	run 4
2		11 ± 1	10 ± 1	
4		18 ± 2	16 ± 2	
24	85 ± 8	85 ± 8	85 ± 8	33 ± 3

[a] The conversion is based on cyclohexanone.

produced in the catalytic reaction (46). In our case, the structure of the clay catalyst may create a suitable environment for the produced alcohol, which can then become an alternative substrate in the neighborhood of the catalytic active site. As in the case of (*Z*)-cyclooctene epoxidation, FeP leaching from the support does not occur, and the blank tests did not reveal any catalytic activity.

The ability of FeP to react with nucleophile NH groups has been studied before by Battioni et al. (47) and Ciuffi et al. (35). These authors have described various approaches to metalloporphyrin immobilization using the sol−gel methodology, all consisting of coordinative binding to ligands attached to a silica support. Battioni et al. (47) reported that a FeP-supported silica system catalyzed the epoxidation of cyclooctene by PhIO with high epoxide yields (>90%), by employing materials with high surface area (about 700 m^2/g) and catalyst loading of 150 mg/g support (15%). The catalytic yields are similar to those achieved with the Ka-FeP catalyst prepared by us, but it may be considered that the catalyst prepared by Battioni et al. (47) has a porphyrin content 5-fold higher than the content in our catalysts Ka-FeP. It is also interesting to note that our catalyst presents a lower surface area (10 m^2/g) compared to the catalysts prepared by other authors.

The surface area and catalyst loading of FeP on the support seems to influence cyclohexane hydroxylation, once this substrate is less reactive. Indeed, Battioni's catalysts are more efficient, 40% of cyclohexanol + cyclohexanone: cf. 30% in the case of Ka-FeP. Our epoxidation results are very similar to those reported by Ciuffi et al. (35) (90%; cf. 85% yields of cyclooctene), in spite of the fact that Ka-FeP presents a lower surface area (10 m^2/g; cf. 140 m^2/g).

As seen from the comparisons, the surface area was not decisive for catalyst performance. These comparisons once again emphasize the influence of the clay matrix in the catalytic system. Unfortunately, no reuse of the catalysts was mentioned in the reports of Battioni et al. (47) or Ciuffi et al. (35). Thus, we can say that our catalyst is economically more viable, because it employs a lower FeP amount and allows catalyst reuse for five consecutive cycles, not to mention the fact that it uses a cheaper matrix, the kaolinite clay.

Because the Ka-FeP system is potentially biomimetic for cytochrome P-450, it seems attractive to test the efficiency of our catalyst in the cyclohexanone Baeyer−Villiger oxidation reaction with H_2O_2 as oxidant, to produce ε-caprolactone (Scheme 1). Table 3 shows that Ka-FeP efficiently

catalyzes the oxidation of cyclohexanone, selectively producing the lactone (85% conversion).

Various blank reactions were carried out, in order to gain information on the behavior of this system. It was observed that some parameters are essential for ketone conversion.

(i) Benzonitrile must be present. As previously observed by Ruiz (48), nitrile acts as an oxygen transfer agent and, in our case, the reaction does not take place when this compound is absent.

(ii) The temperature is a decisive factor. The catalytic tests were carried out at room temperature and at 60 and 80 °C, and the best conversion results were achieved at 80 °C (85%; cf. 40 % conversion of cyclohexanone in ε-caprolactone).

(iii) In the absence of FeP and using the solid Ka-et (blank test) as catalyst, there is no formation of ε-caprolactone, once again demonstrating that FeP plays a fundamental role in oxygen transfer.

To ensure that FeP really acts in the process of oxygen transfer, this catalyst was reacted with excess imidazole prior to the BV reaction. It is well established that the pentafluorophenyl-substituted FeP tends to bis-coordinate to nitrogen bases, which can result in the formation of low-spin Fe(III) or in the reduction of Fe(III) to Fe(II). It has been previously observed that Me(III)P reduction to Me(II)P can occur during the preparation of catalysts through the sol−gel process in the presence of a nitrogen base catalyst, thereby leading to materials with low catalytic activity (35). In our case, as expected, the conversion observed in the BV reaction is drastically reduced in the presence of excess imidazole, confirming the participation of FeP in the oxygen transfer. The results were largely dependent on the reaction time; the highest conversion, 85% of ε-caprolactone, was achieved after 24 h. This can be explained by the localization of FeP in the clay interlayer region which, despite being disordered, may render the access of the substrate to the catalyst and the further diffusion of the products difficult. It can again be remarked that all the reactions involved herein proceed by a typical heterogeneous catalysis mechanism, since FeP did not leach from the support during the entire process.

Zhou et al. (49) pioneered the use of iron porphyrins as catalyst in the Baeyer−Villiger reaction. They described the efficient selective BV reaction of ketones to lactones catalyzed by [*meso*-tetraphenylporphinato]iron(III), Fe(TPP), using dioxygen as oxidant, in a homogeneous system. High lactone conversion (96%) was obtained by these authors. Although our results are lower than that reported by these authors (85%), it is possible to reuse our catalyst, which once more demonstrates its economic viability.

The catalyst reuse was available in the oxidation reaction (Table 3) using hydrogen peroxide as oxidant. The catalysts were separated from the reaction mixture after each experiment by simple filtration and dried before being used in the subsequent run. Good conversions, 85%, were obtained for the first three reuses. However, after the third reuse, it was very difficult to dry the used catalyst because it was converted into a gel-type solid. Once dried, the catalyst was used for a new catalytic cycle, but the conversion strongly decreased to 33%. It is remarkable that, even after this fourth use, no leaching was observed. New studies must be carried out to explain the transformation of the catalyst into a gel-like solid after three catalytic cycles.

SUMMARY AND CONCLUSIONS

Natural kaolinite is an excellent candidate for organofunctionalization, and it has been effectively functionalized with synthetic second-generation iron porphyrin. The immobilization process is very simple and allows for the preparation of an efficient catalyst for various oxidation reactions. This catalyst is more active than comparable homogeneous counterparts. It seems that both reactants can easily access the active sites, and product diffusion is easier compared with similar silica and aluminosilicate systems. The layer structure of the support resulted in good maintenance of its properties. Even under various catalytic cycles, problems related to the diffusion of the reactants to the active sites or of the products out of the catalyst were not observed, in contrast with what is observed for other supports, such as silicas and aluminas.

Iodosylbenzene was successfully employed in (*Z*)-cyclooctene epoxidation. The catalyst was reused up to five times without any decrease in yield. Hydrogen peroxide, a clean oxidant, was also successfully used in the conversion of cyclohexanone into ϵ-caprolactone, the so-called Baeyer−Villiger reaction. Conversion of 85% showed the catalytic ability of the system. To the best of our knowledge, this is the first work describing the Baeyer−Villiger reaction catalyzed by a heterogeneous iron porphyrin and reporting the reuse of the catalyst. Thus, the preparation of kaolinite-based compounds enables the large-scale use of iron porphyrins, usually expensive catalysts, enabling its reuse. In conclusion, a relatively inexpensive, largely selective, reusable oxidation catalyst has been prepared.

Acknowledgment. This work has been carried out in the framework of an Interuniversity Cooperation Project between the Spanish and Brazilian Ministries of Education (references PHB2005-0077-PC and CAPES 110/06). The Spanish authors acknowledge financial support from the *Ministerio de Ciencia e Innovación* (reference MAT2007-66439-C02) and the *Junta de Castilla y León* (reference SA101A07). R.T. acknowledges financial support from the *MEC* through the *Ramon-y-Cajal* program. The Brazilian group acknowledges support from the FAPESP and CNPq.

Supporting Information Available: Text, figures, and a table giving details of the purification of natural kaolin, characterization of the purified kaolinite, and characterization of the kaolinite−DMSO complex. This material is available free of charge via the Internet at http://pubs.acs.org.

REFERENCES AND NOTES

(1) Que, L., Jr.; Tolman, W. B. *Nature* **2008**, *455*, 333–340.
(2) Mansuy, D. *C. R. Chim.* **2007**, *10*, 392–413.
(3) Mansuy, D. *Catal. Today* **2008**, *138*, 2–8.

(4) Schiavon, M. A.; Iamamoto, Y.; Nascimento, O. R.; Assis, M. D. D. *J. Mol. Catal. A: Chem.* **2001**, *174*, 213–222.
(5) Mansuy, D. *Coord. Chem. Rev.* **1993**, *125*, 129–142.
(6) de Lima, O. J.; de Aguirre, D. P.; de Oliveira, D. C.; Silva, M. A.; Mello, C.; Leite, C. A. P.; Sacco, H. C.; Ciuffi, K. J. *J. Mater. Chem.* **2001**, *11*, 2476–2481.
(7) Huang, G.; Liu, S.-Y.; Guo, Y.-A.; Wang, A. -P.; Luo, J.; Cai, C.-C. *Appl. Catal. A* **2009**, *358*, 173–179.
(8) Kameyama, H.; Narumi, F.; Hattori, T.; Kameyama, H. *J. Mol. Catal. A: Chem.* **2006**, *258*, 172–177.
(9) Barbara, P.; Liguori, F. *Chem. Rev.* **2009**, *109*, 515–529.
(10) Papacídero, A. T.; Rocha, L. A.; Caetano, B. L.; Molina, E.; Sacco, H. C.; Nassar, E. J.; Martinelli, Y.; Mello, C.; Nakagaki, S.; Ciuffi, K. J. *Colloids Surf., A* **2006**, *275*, 27–35.
(11) Suslick, K. S.; Bhyrappa, P.; Chou, J. -H.; Kosal, M. E.; Nakagaki, S.; Smithenry, D. W.; Wilson, S. R. *Acc. Chem. Res.* **2005**, *38*, 283–291.
(12) McDonald, A. R.; Franssen, N.; van Klink, G. P. M.; van Koten, G. *J. Organomet. Chem.* **2009**, *694*, 2153–2162.
(13) Letaief, S.; Detellier, C. *Can. J. Chem.* **2008**, *86*, 1–6.
(14) ten Brink, G.-J.; Arends, I. W. C. E.; Sheldon, R. A. *Chem. Rev.* **2004**, *104*, 4105–4123.
(15) Leak, D. J.; Sheldon, R. A.; Woodley, J. M.; Adlercreutz, P. *Biocatal. Biotransform.* **2009**, *27*, 1–26.
(16) Corma, A.; Nemeth, L. T.; Renz, M.; Valencia, S. *Nature* **2001**, *412*, 423–425.
(17) Steffen, R. A.; Teixeira, S.; Sepulveda, J.; Rinaldi, R.; Schuchardt, U. *J. Mol. Catal. A: Chem.* **2008**, *287*, 41–44.
(18) Frost, R. L.; Kristof, J.; Horvath, E.; Kloprogge, J. T. *J. Phys. Chem. A* **1999**, *103*, 9654–9660.
(19) Itagaki, T.; Kuroda, K. *J. Mater. Chem.* **2003**, *13*, 1064–1068.
(20) de Faria, E. H.; Lima, O. J.; Ciuffi, K. J.; Nassar, E. J.; Vicente, M. A.; Trujillano, R.; Calefi, P. S. *J. Colloid Interface Sci.* **2009**, *335*, 210–215.
(21) Tunney, J. J.; Detellier, C. *Can. J. Chem.* **1997**, *75*, 1766–1772.
(22) Letaief, S.; Detellier, C. *Chem. Commun.* **2007**, 2613–2615.
(23) Lindsey, J. S.; Schreiman, I. C.; Hsu, H. C.; Kearney, P. C.; Marguerettaz, A. M. *J. Org. Chem.* **1987**, *52*, 827–836.
(24) Adler, A. D.; Longo, F. R.; Kampas, F.; Kim, J. *J. Inorg. Nucl. Chem.* **1970**, *32*, 2443–2445.
(25) Brunauer, S.; Emmett, P. H.; Teller, E. *J. Am. Chem. Soc.* **1938**, *60*, 309–319.
(26) Sharefkin, J. G.; Saltzmann, H. *Org. Synth.* **1963**, *43*, 62–64.
(27) Lucas, H. J.; Kennedy, E. R.; Forno, M. W. *Org. Synth.* **1963**, *43*, 483.
(28) Iamamoto, Y.; Prado, C. M. C.; Sacco, H. C.; Ciuffi, K. J.; Assis, M.; Maestrin, A. P. J.; Melo, A. J. B.; Baffa, O.; Nascimento, O. R. *J. Mol. Catal. A: Chem.* **1997**, *117*, 259–271.
(29) Belver, C.; Bañares-Muñoz, M. A.; Vicente, M. A. *Chem. Mater.* **2002**, *14*, 2033–2043.
(30) Tunney, J. J.; Detellier, C. *Chem. Mater.* **1993**, *5*, 747–748.
(31) Brandt, K. B.; Elbokl, T. A.; Detellier, C. *J. Mater. Chem.* **2003**, *13*, 2566–2572.
(32) Tonlé, I. K.; Diaco, T.; Ngmeni, E.; Detellier, C. *Chem. Mater.* **2007**, *26*, 6629–6636.
(33) Wypych, F.; Satyanarayana, K. G. In *Clay Surfaces: Fundamentals and Application*, 1st ed.; Wypych, F., Ed.; Elsevier Science/Academic Press: Amsterdam, 2004; Vol. 1, p 32.
(34) Mansuy, D.; Battioni, P. In *Metalloporphyrins in Catalytic Oxidations*, 1st ed.; Sheldon, R. A., Ed.; Marcel Dekker: New York, 1994; Vol. 1, p 99.
(35) Ciuffi, K. J.; Biazzotto, J.; Sacco, H. C.; Vidoto, E. A.; Nascimento, O. R.; Serra, O. A.; Iamamoto, Y. *J. Non-Cryst. Solids* **2000**, *273*, 100–108.
(36) Smith, K. M. In *Porphyrins and Metalloporphyrins*; 1st ed.; Smith, K. M., Ed.; Elsevier/North-Holland Biomedical Press: Amsterdam, 1975; Vol. 1, p 21.
(37) Nakagaki, S.; Machado, G. S.; Halma, M.; Marangon, A. A. S.; Castro, K. A. D. F.; Mattoso, N.; Wypych, F. *J. Catal.* **2006**, *242*, 110–117.
(38) Lombardi, K. C.; Guimarães, J. L.; Mangrich, A. S.; Mattoso, N.; Abatte, M.; Schreiner, W. H.; Wypych, F. *J. Braz. Chem. Soc.* **2002**, *13*, 270–275.
(39) Gardolinski, J. E.; Peralta-Zamora, P.; Wypych, F. *J. Colloid Interface Sci.* **1999**, *211*, 137–141.
(40) Breen, C. *Clay Miner.* **1991**, *26*, 487–496.
(41) Ciuffi, K. J.; Nassar, E. J.; Rocha, L. A.; da Rocha, Z. N.; Nakagaki, S.; Mata, G.; Trujillano, R.; Vicente, M. A.; Korili, S. A.; Gil, A. *Appl. Catal., A* **2007**, *319*, 153–162.
(42) Groves, J. T. *J. Inorg. Biochem.* **2006**, *100*, 434–447.
(43) Sacco, H. C.; Iamamoto, Y.; Lindsay Smith, J. R. *J. Chem. Soc., Perkin Trans. 2* **2001**, 181–190.
(44) Schuchardt, U.; Carvalho, W. A.; Spinacé, E. V. *Synlett* **1993**, *10*, 713–718.
(45) Nunes, G. S.; Mayer, I.; Toma, H. E.; Araki, K. *J. Catal.* **2005**, *236*, 55–61.
(46) Inchley, P.; Lindsay Smith, J. R.; Lower, R. J. *New J. Chem.* **1989**, *13*, 669–676.
(47) Battioni, P.; Cardin, E.; Louloudi, M.; Schöllhorn, B.; Spyroulias, G. A.; Mansuy, D.; Traylor, T. G. *Chem. Commun.* **1996**, *17*, 2037–2038.
(48) Ruiz, J. R.; Jiménez-Sanchidrián, C.; Llamas, R. *Tetrahedron* **2007**, *63*, 1435–1439.
(49) Zhou, X.-T.; Ji, H.-B.; Yuan, Q.-L. *J. Porphyrins Phthalocyanines* **2008**, *12*, 94–100.

AM900556B